Dalitz Plot Analysis

Author: Javier Fernández Martín
Facultat de Física, Universitat de Barcelona, Diagonal 645, 08028 Barcelona, Spain.

Advisors: Vincent Mathieu, Iñigo Asiáin

Abstract: The reaction $p + \pi^0 \to \eta + \pi^0 + p$ is analyzed using Dalitz and Van Hove plots, comparing their ability to resolve resonances. Using Monte Carlo simulations with uniform and resonant amplitudes, it is demonstrated that Van Hove plots provide superior resonance separation and more precise measurements of resonance features —mass and width—. This establishes Van Hove plots as a powerful tool for analyzing complex resonance structures in high-energy processes.
Keywords: High Energy Physics, Resonance Phenomena, Kinematic Analysis and Data Analysis.
SDGs: Clean and sustainable energy, and Industry, Innovation and Infrastructure.

I. INTRODUCTION

The study of three-body decays provides a powerful tool for investigating resonance structures and dynamics in particle collisions. Resonances are short-lived intermediate states that decay into final-state particles, and in such processes, the Dalitz plot provides a graphical representation of the phase-space distribution, where resonance bands appear as regions with a high concentration of events. These bands come from the quantum mechanical transition amplitudes, which carry the probability of the system evolving from the initial to the final-state. The differential cross-section for a three-body decay is proportional to the squared transition amplitude [1]:

$$\frac{d\sigma}{ds_{12}ds_{23}} \propto |\mathcal{A}|^2, \tag{1}$$

where s_{12} and s_{23} are Mandelstam invariants for pair of particles. However, while the Dalitz plot has been widely used, it is limited by resonance overlaps, complicating the isolation of individual processes. This situation is overcome with the Van Hove plot.

In this work, I present a comparison of Dalitz and Van Hove plot methodologies, analyzing multiple decay channels in the reaction:

$$p + \pi^0 \to \eta + \pi^0 + p$$

All analyses are performed in the center of mass (COM) frame, where the total momentum of the system is zero. In this reaction, the final-state can originate from intermediate resonances, such as the mesons a_2 and N^*, and the baryon Δ. The corresponding decay channels are: $a_2 \to \eta + \pi^0$, $N^* \to \eta + p$, and $\Delta \to \pi^0 + p$.

This TFG is organized as follows. First, I introduce the Dalitz and Van Hove plot frameworks. Next, I explain the event generation methodology used to obtain the results. Finally, I present and compare the results derived from the Dalitz and Van Hove methods. The goal of this work is to establish the Van Hove plot as a more robust framework for resonance studies in three-body decays.

II. DALITZ PLOT BASIS

For a generic reaction $A + B \to 1 + 2 + 3$, the phase-space distribution can be visualized using a Dalitz plot. The Dalitz plot is a graphical representation of the squared invariant masses s_{12} and s_{23}, where kinematically possible events are displayed. For a pair of final-state particles i and j, the squared invariant mass is defined as [2]:

$$s_{ij} = (p_i^\mu + p_j^\mu)^2 = m_i^2 + m_j^2 + 2E_iE_j - 2|\vec{p}_i||\vec{p}_j|\cos\theta_{ij}, \tag{2}$$

Here, $p_i^\mu = (E_i,\, \vec{p_i})$, is the four-momentum of the final-state particle i. The, invariant squared masses s_{ij} are constrained by energy-moment conservation, satisfying [2]:

$$s_{12} + s_{13} + s_{23} = M^2 + m_1^2 + m_2^2 + m_3^2, \tag{3}$$

where $M^2 \equiv s$ is the invariant squared mass of the initial system, defined as $s = (p_A + p_B)^2$. It is also important to define another Mandelstam invariants: $t_i = (p_A - p_i)^2$ and $u_i = (p_B - p_i)^2$, for a final-state particle.

As it is reflected in Fig. 1, the boundaries of the Dalitz plot are determined by the allowed range of s_{23} for a fixed s_{12}. From Eq.(2), these limits occur when the momenta of particles 2 and 3 are aligned or anti-aligned [1]:

$$s_{23}^{\pm} = (E_2 + E_3)^2 - \left(\sqrt{E_2^2 - m_2^2} \mp \sqrt{E_3^2 - m_3^2}\right)^2, \tag{4}$$

where $s_{23}^{\pm}$ are the kinematic limits for fixed s_{12}, with $\pm$ sign corresponding to $\cos\theta_{23} = \mp 1$ in Eq.(2). $E_{2,3}$ are the energies of particles 2 and 3, related to s_{ij} via [2]:

$$E_i = \frac{s + m_i^2 - s_{jk}}{2\sqrt{s}} \quad (i, j, k) \in \text{perm}(1, 2, 3). \tag{5}$$

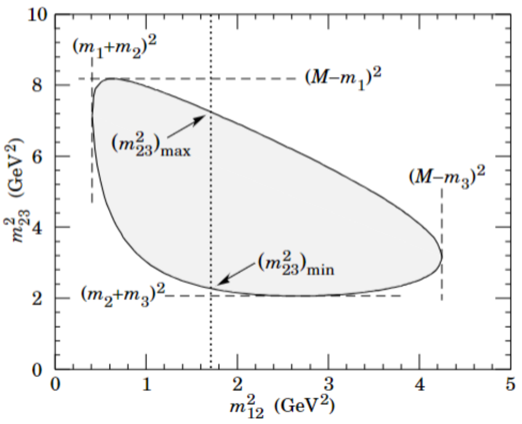

FIG. 1: Dalitz plot for a three-body decay in the (s_{12}, s_{23}) plane, where the axes represent the squared invariant squared masses $s_{12} \equiv m_{12}^2$ and $s_{23} \equiv m_{23}^2$. The kinematic boundaries of the plot are determined by energy-momentum conservation. Taken from Ref.[1].

III. VAN HOVE PLOT BASIS

In high-energy hadron collisions, transverse momentum typically remain small, allowing us to decouple phase-space into longitudinal and transverse components. The longitudinal momentum refers to the direction of a particle along the beam axis (z-axis in our choice), while the transverse momentum are the perpendicular components to the beam axis. The momentum of a particle can be defined as [3]:

$$\vec{p_i} = \vec{q_i} + \vec{r_i}, \tag{6}$$

where $\vec{q_i}$ and $\vec{r_i}$ are the longitudinal and transverse momenta respectively, and both satisfy momentum conservation. The energy is defined as [3]:

$$E_i = \sqrt{m_i^2 + r_i^2 + q_i^2} = \sqrt{{m'_i}^2 + q_i^2}, \tag{7}$$

where m'_i is the effective mass for longitudinal motion ($m'_i = \sqrt{m_i^2 + r_i^2}$), $q_i^2 = |\vec{q_i}|^2$ and $r_i^2 = |\vec{r_i}|^2$. Energy conservation imposes [3]:

$$M = \sum_{i=1}^{3} E_i, \tag{8}$$

where M is the total energy of the initial system. Following the discussion in [3], each collision maps to a point (q_1, q_2, q_3) in a 3D Euclidean space S_3, but the momentum conservation restricts these points to a 2D plane L_2, known as the longitudinal phase-space, defined by $\sum_i \vec{q_i} = 0$. Thus, solving numerically Eq.(8), with some additional considerations that will be explained later, it will be possible to construct the Van Hove plot as the one in Fig. 2.

For fixed $\vec{r_i}$ (and then fixed m'_i), the points (q_1, q_2, q_3) lie on a 1D surface K_1 within L_2.

In the massless limit, the total energy in Eq.(8) simplifies to [3]:

$$M = \sum_{i=1}^{3} |q_i|, \tag{9}$$

defining a hexagonal polyhedron H_1 in L_2. Alternatively, for $q_i^2 \ll {m'_i}^2$, a Taylor expansion can be done in Eq.(7) [3]:

$$\sqrt{{m'_i}^2 + q_i^2} \approx m'_i + \frac{q_i^2}{2m'_i}, \tag{10}$$

so that the total energy in Eq.(8) will be affected, demonstrating that K_1 deviates from H_1, i.e., its sides and vertices become rounded, with a curvature that depends on m'_i (i.e., on m_i and $\vec{r_i}$). Notably, for $\vec{r_i}$ negligible, then K_1 always lies inside H_1, and for non negligible $\vec{r_i}$, K_1 is strictly contained within the $\vec{r_i}$ negligible case. This can be seen in Fig. 2. The longitudinal momentum of each particle are expressed in polar coordinates, leaving only dependencies in the angle (ω) and radius (q) [3]:

$$\begin{aligned} q_1 &= \sqrt{\frac{2}{3}} q \sin\omega, \quad q_2 = \sqrt{\frac{2}{3}} q \sin\left(\omega - \frac{2\pi}{3}\right), \\ q_3 &= \sqrt{\frac{2}{3}} q \sin\left(\omega - \frac{4\pi}{3}\right), \end{aligned} \tag{11}$$

where $q = \sqrt{q_1^2 + q_2^2 + q_3^2}$ and $\omega \in [0, 2\pi]$.

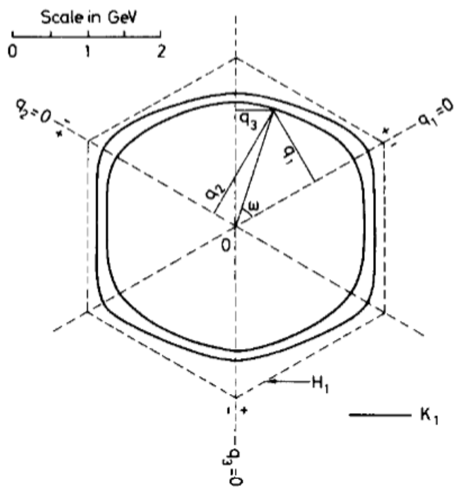

FIG. 2: Longitudinal phase-space for a $\pi\pi N$ final-state system. The inner full curve is K_1 for non negligible $\vec{r_i}$ and the outer one is K_1 for $\vec{r_i}$ negligible. The dashed line is the hexagon H_1. The axes q_1, q_2 and q_3, represent the longitudinal momentum of the particles and the signs + and − of each axis correspond to the direction of the associated particle. Taken from Ref.[3].

A. Structure of the Longitudinal Phase-Space

The distribution of events along the Van Hove plot is influenced by how the available momentum is shared among particles. In particular, certain configurations lead to an increase in the event density. The density of events is determined by the following expression [3]:

$$D_N \approx \frac{M}{\left(\sum_{i=1}^{3} |\gamma_i|\right)^2} \ , \tag{12}$$

where γ_i are the directional cosines of each particle's longitudinal momentum in Eq.(11), satisfying $\sum_{i=1}^{3} \gamma_i^2 = 1$, and M is the total energy of the initial system.

Eq.(12) shows that the event density is enhanced when $\sum |\gamma_i|$ is minimized, i.e., when the longitudinal momenta are highly unbalanced. For three particles, the minimum occurs when one particle carries negligible longitudinal momentum ($\vec{q_1} \approx 0$) while the other two are equal and opposite ($\vec{q_2} = -\vec{q_3}$).

According to Fig. 3 and the preceding analysis, in the Van Hove plot these configurations correspond to angles ω that are multiples of 60, coinciding with the hexagon axes where D_N is maximized.

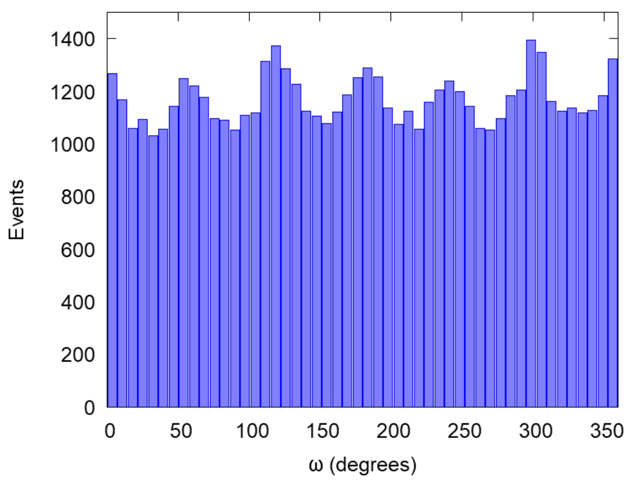

FIG. 3: Event density peaks in the Van Hove plot for the reaction $p + \pi^0 \to \eta + \pi^0 + p$ at $\sqrt{s} = 14$ GeV, occurring at angles $\omega = 60k$ (degrees), where $k = 0, 1, \ldots, 6$, which coincide with the axes of the Van Hove plot.

IV. EVENT GENERATION METHODOLOGY

The methodology for the event generation was carried out by me, implementing a Fortran simulation. First of all, the program creates the phase-space where $|\mathcal{A}|^2 = 1$. Once this phase-space is created, the program will be extended to scenarios where $|\mathcal{A}|^2 \neq 1$.

A. Phase-Space Generation for $|\mathcal{A}|^2 = 1$

First of all, the allowed kinematical region is created for the Dalitz plot. Hence, given the total energy M and the masses of the final-state particles m_1, m_2 and m_3, the program must generate uniform random values for the squared invariant squared masses s_{12} and s_{23}. The allowed values for s_{12} and s_{23} are determined by M, m_1, m_2 and m_3, as it is shown in Fig. 1. Since there is no kinematic boundary conditions applied, the result of the phase-space will be a square where the events are uniformly distributed. Once this uniform square is created, the kinematic boundary conditions are applied following Eq.(4). This will make decrease the number of events generated initially. Also the value of s_{13} is calculated using Eq.(3).

Second, the four-momentum of the final-state particles are constructed. For this step, the initial beam direction must be specified; in this case, the z-axis is chosen as the beam axis. Consequently, the four-momentum are initially constructed in the $X-Y$ plane using the modules of the momentum of each particle ($|\vec{p_i}| = \sqrt{E_i^2 - m_i^2}$). The energy associated to each particle is calculated with Eq.(5). The four-momentum in the plane are:

$$\begin{aligned} p_1^\mu &= (E_1, p_1, 0, 0), \\ p_2^\mu &= (E_2, p_2 \cos\theta_{12}, p_2 \sin\theta_{12}, 0), \\ p_3^\mu &= (E_3, -(p_{1,x} + p_{2,x}), -p_{2,y}, 0), \end{aligned} \tag{13}$$

where the angle θ_{12} is calculated in Eq.(2). This ensures momentum conservation $\sum_i \vec{p_i} = 0$. Later, Euler rotations in arbitrary directions are applied to the $X-Y$ planes to ensure isotropy among the events:

$$p_i' = R_z(\phi) R_y(\theta) p_i, \tag{14}$$

where $\phi \in [0, 2\pi]$ and $\theta \in [0, \pi]$. Using Eq.(11), it is possible to calculate the radius (q) and the angle (ω), which are used for the construction of the Van Hove plot.

The kinematic limits of the Dalitz plot are determined by Eq.(4), which defines the allowed range of s_{23} for a fixed s_{12}. In the Van Hove plot, these limits split into two boundaries: the inner boundary in Eq.(8), dependent to masses and longitudinal momenta of the particles, and the outer boundary in Eq.(9), where only longitudinal momenta contributes in the total energy. Both boundaries are solved numerically via the secant method, with the longitudinal momentum of each particle expressed in the polar coordinates of Eq.(11).

B. Phase-Space Generation for $|\mathcal{A}|^2 \neq 1$

For non-constant transition amplitudes, one must begin where the $|\mathcal{A}|^2 = 1$ case concludes, and extend the Monte Carlo approach using $|\mathcal{A}|^2 \neq 1$. For the extension of the Monte Carlo approach, the method implemented is an acceptance-rejection algorithm, where $|\mathcal{A}|^2$ is used to distribute the generated events. This is necessary in order to correctly sample events.

For the case is being studied, the transition amplitude incorporates three resonant contributions:

$$\mathcal{A} = \mathcal{A}_{a_2} + \mathcal{A}_{N^*} + \mathcal{A}_{\Delta} \equiv \sum_i \mathcal{A}_i(s_{jk}, x), \qquad (15)$$

where s_{jk} is the invariant squared mass associated with the pair of final-state particles involved in the resonance, and x refers to other kinematic variables like u_p, t_{π^0} or t_η, depending on the resonance. Each transition amplitude follows a function of the Breit-Wigner form:

$$\mathcal{A}_i(s_{jk}, n_i) = \frac{s^{n_i}}{s_{jk} - m_i^2 + i m_i \Gamma_i}, \qquad (16)$$

where m_i and Γ_i are the mass and width, respectively, of the resonance in each channel, s is the squared total energy and n_i is a fitted exponent related to the resonance channel which contain the kinematic variables associated to x, presented in Eq.(15). The fixed parameters used are:

TABLE I: Experimental mass and width values of the resonances in each channel taken from Ref.[1].

Resonance	Mass (GeV)	Width (GeV)
a_2	1.320	0.103
N^*	1.520	0.115
Δ	1.232	0.120

Finally, I explain how the acceptance-rejection algorithm works. Once the phase-space is generated for $|\mathcal{A}|^2 = 1$, the non-constant transition amplitude of the reaction is defined. Then, the physical amplitude $|\mathcal{A}|^2$ is evaluated for each event. The algorithm proceeds by first identifying the maximum value of $|\mathcal{A}|^2$ across all the events generated. This value is increased by a 10% safety margin to ensure complete coverage of the amplitude range. For each event, a uniform random number P between zero and this adjusted maximum is generated. The event is accepted if the value $|\mathcal{A}|^2$ of the specific event falls below P. This guarantees that the distribution of events follows the physical dynamics that encodes $|\mathcal{A}|^2$. Additionally, the algorithm will be asked to ensure there is the number of events required, repeating the process many times as needed.

V. RESULTS

In this section, the results obtained for the Fig. 4, are presented. This energy is chosen at a lower center of mass energy of the initial system ($\sqrt{s} = 2.65$ GeV). This is because resonance bands can be seen clearly than at higher energies, where the events tend to spread over a higher range over the s_{12} and s_{23} axes, making the resonance bands more difficult to identify.

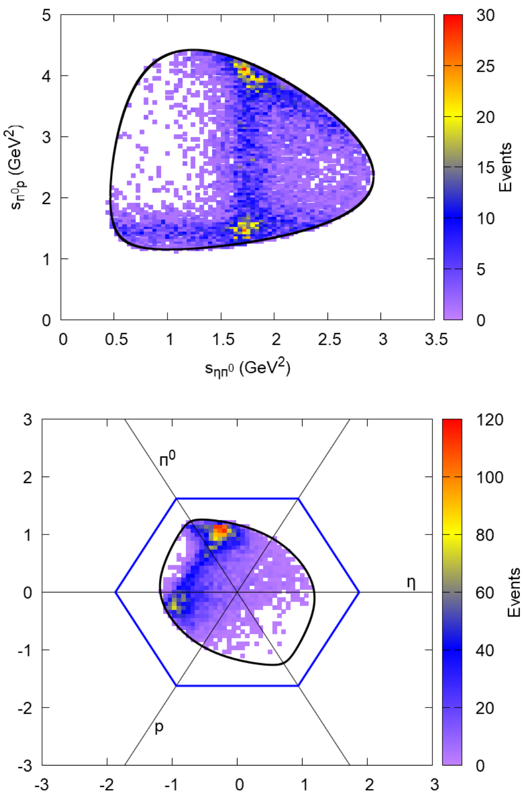

FIG. 4: (a) Top: Dalitz plot heatmap image for the reaction $p + \pi^0 \to \eta + \pi^0 + p$, at $\sqrt{s} = 2.65$ GeV. Clear resonant structures appear as bands, corresponding to intermediate resonant states near their characteristic squared mass values. (b) Bottom: Van Hove plot heatmap image for the reaction $p + \pi^0 \to \eta + \pi^0 + p$, at $\sqrt{s} = 2.65$ GeV. Distinct resonance structures are observed, characterized by particular configurations of the longitudinal momenta of the final-state particles. The scale is in GeV as in Fig. 2

Having generated the Dalitz and Van Hove distributions in Fig. 4, the methods are compared by projecting their event densities onto the invariant squared mass axis of the studied decay channel. The analysis focuses on specific regions of the Van Hove plot that exhibit resonant structures, especially those where longitudinal momentum distributions reveal characteristic features of the decay process. Therefore, taking advantage of geometry properties from the Van Hove plot, our program use the angle ω to select the data where the resonance is occurring. In contrast, the Dalitz plot cuts data by selecting events from other resonances, artificially increasing the event count for that channel.

Using both methods, it is easy to see that the Dalitz plot is affected by background and overlapping contributions from other resonances. In contrast, the Van Hove plot helps when revealing the real quantity of events in the resonance.

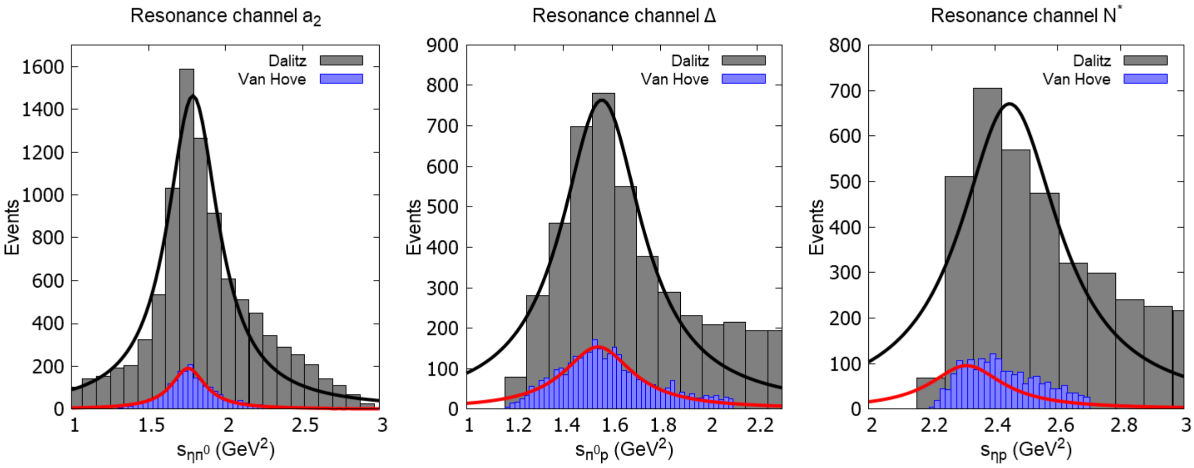

FIG. 5: Histograms of event distributions obtained using the Dalitz and Van Hove methods, shown for the three channels at $\sqrt{s} = 2.65$ GeV. The superimposed lines represent Breit-Wigner fits: black for Dalitz and red for Van Hove.

Finally, the mass and width of the resonant particles involved are calculated for both methods using the Breit-Wigner fits in Fig. 5

TABLE II: Measured mass and width values of the resonant states involved, obtained through fits to the invariant squared mass distributions shown in Fig. 5.

Resonance	Method	Mass (GeV)	Width (GeV)
a_2	Dalitz Plot	1.336 ± 0.004	0.151 ± 0.011
	Van Hove plot	1.325 ± 0.001	0.100 ± 0.003
N^*	Dalitz Plot	1.564 ± 0.009	0.122 ± 0.029
	Van Hove plot	1.546 ± 0.002	0.095 ± 0.006
Δ	Dalitz Plot	1.248 ± 0.007	0.162 ± 0.022
	Van Hove plot	1.241 ± 0.002	0.140 ± 0.006

In Table II, both methods give consistent results for the mass determination; however, the Van Hove method shows a modest improvement in the precision over the Dalitz plot analysis. This improvement becomes more evident in the determination of the resonance width, where the Van Hove plot significantly reduces background contributions. Overall, the results in Table II agree with Table I, but the Van Hove method provides better precision than the Dalitz plot analysis.

It is important to mention that at higher energies ($\sqrt{s}$), the results would deviate from the theoretical values shown in Table I as the energy increase. This is because it becomes more difficult to identify the resonances, since the events are spread over a wider kinematic range, making data selection more challenging.

VI. CONCLUSIONS

This study demonstrates that the combined use of the Dalitz and Van Hove plot, provides a more comprehensive understanding of the reaction dynamics and band resonances in a collision of particles. Although, the Dalitz plot indeed reveals resonant structures through invariant squared mass correlations, it is affected by resonance overlap, which can hinder the determination of resonance parameters. Then, by applying a targeted selection of events based on the Van Hove plot, it is possible to isolate specific kinematic regions and reduce these background effects, obtaining more accurate results for these resonance parameters.

VII. ACKNOWLEDGMENTS

I am deeply thankful to my tutor Vincent Mathieu for his guidance and patience. I also would like to thank Iñigo Asiáin, who helped me overcome many problems during the research of my TFG. I am especially thankful to my family, who have been always supporting me.

[1] S. Navas *et al.*, "Review of particle physics," *Phys. Rev. D*, vol. 110, no. 3, p. 030001, 2024.
[2] E. Byckling and K. Kajantie, *Particle Kinematics*. A Wiley-Interscience publication, Wiley, 1973.
[3] L. Van Hove, "Longitudinal phase-space plots of multiparticle hadron collisions at high energy," *Nuclear Physics B*, vol. 9, no. 3, pp. 331–348, 1969.

Anàlisi del Diagrama de Dalitz

Author: Javier Fernández Martín
Facultat de Física, Universitat de Barcelona, Diagonal 645, 08028 Barcelona, Spain.

Advisors: Vincent Mathieu, Iñigo Asiáin

Resum: La reacció $p + \pi^0 \rightarrow \eta + \pi^0 + p$ s'analitza utilitzant diagrames de Dalitz i de Van Hove, comparant-ne la capacitat per resoldre ressonàncies. Mitjançant simulacions de Monte Carlo amb amplituds uniforms i ressonants, es demostra que els diagrames de Van Hove proporcionen una separació de ressonàncies superior i mesures més precises de les característiques de les ressonàncies—massa i amplada—. Això estableix els diagrames de Van Hove com una eina potent per analitzar estructures de ressonància complexes en processos d'alta energia.
Paraules clau: Física d'Altes Energies, Fenòmens Resonants, Anàlisi Cinemàtica i Anàlisi de Dades.
ODSs: Energia neta i sostenible, i Indústria, innovació i infraestructuras.

Objectius de Desenvolupament Sostenible (ODSs o SDGs)

1. Fi de la es desigualtats		10. Reducció de les desigualtats	
2. Fam zero		11. Ciutats i comunitats sostenibles	
3. Salut i benestar		12. Consum i producció responsables	
4. Educació de qualitat		13. Acció climàtica	
5. Igualtat de gènere		14. Vida submarina	
6. Aigua neta i sanejament		15. Vida terrestre	
7. Energia neta i sostenible	X	16. Pau, justícia i institucions sòlides	
8. Treball digne i creixement econòmic		17. Aliança pels objectius	
9. Indústria, innovació, infraestructures	X		

El contingut d'aquest TFG, part d'un grau universitari de Física, es relaciona amb l'ODS 7, i en particular amb la fita 7.1 perquè pot promoure la cooperació internacional per a facilitar l'accés a la investigació d'energía neta. També es pot relacionar amb l'ODS 9, i en particular amb la fita 9.5, perquè pot promoure la investigació científica.